Comput Mech (2013) 52:631–648
DOI 10.1007/s00466-013-0836-9

ORIGINAL PAPER

A wideband FMBEM for 2D acoustic design sensitivity analysis based on direct differentiation method

Leilei Chen · Changjun Zheng · Haibo Chen

Received: 2 June 2012 / Accepted: 13 January 2013 / Published online: 30 January 2013

Abstract This paper presents a wideband fast multipole boundary element method (FMBEM) for two dimensional acoustic design sensitivity analysis based on the direct differentiation method. The wideband fast multipole method (FMM) formed by combining the original FMM and the diagonal form FMM is used to accelerate the matrix-vector products in the boundary element analysis. The Burton–Miller formulation is used to overcome the fictitious frequency problem when using a single Helmholtz boundary integral equation for exterior boundary-value problems. The strongly singular and hypersingular integrals in the sensitivity equations can be evaluated explicitly and directly by using the piecewise constant discretization. The iterative solver GMRES is applied to accelerate the solution of the linear system of equations. A set of optimal parameters for the wideband FMBEM design sensitivity analysis are obtained by observing the performances of the wideband FMM algorithm in terms of computing time and memory usage. Numerical examples are presented to demonstrate the efficiency and validity of the proposed algorithm.

Keywords Design sensitivity analysis · Wideband FMBEM · Burton–Miller method · Direct differentiation method

L. Chen · C. Zheng · H. Chen (✉)
Department of Modern Mechanics, University of Science and Technology of China, Hefei 230027, Anhui, People's Republic of China
e-mail: hbchen@ustc.edu.cn

C. Zheng
e-mail: cjzheng@mail.ustc.edu.cn

L. Chen
e-mail: chenllei@mail.ustc.edu.cn

1 Introduction

Acoustic design sensitivity analysis can provide information on how the geometry change affecting the acoustic performance of the given structure, and it is a key step of the acoustic optimization process. Both the finite element method [1,2] and the boundary element method (BEM) can be used to implement the sensitivity analysis. It is well-known that BEM has been widely used to solve the acoustic problems, because it provides an excellent accuracy and easy mesh generation. In particular, for exterior acoustic problems, the Sommerfeld radiation condition [3] at infinity is automatically satisfied. In BEM implementation, the Galerkin method has been widely applied to the numerical solution of boundary integral equation [4,5], and it provides a powerful theoretical background for this method. Traditionally, however, the collocation method was widely used in the engineering community and is adopted in this research.

Acoustic design sensitivity formulations presented in this paper are obtained by differentiating the boundary integral equations with respect to design variables which determine the contour of the structure. A number of related researches can be found in 1990s. Smith and Bernhard [6] derived the semi-analytical sensitivity formulation by differentiating the discretized boundary integral equation. Matsumoto et al. [7,8], Koo et al. [9] and Kane et al. [10] derived different acoustic sensitivity expressions with respect to the shape design variables. However, the intrinsic drawback of the conventional BEM has prevented the above sensitivity algorithms to large scale engineering problems. In general, the BEM discretizes the boundary instead of the domain and takes less difficulties due to the one-dimension reduction in mesh generation. However, it produces a dense and non-symmetrical coefficient matrix, which induces $O(N^3)$ arithmetic operations to solve the system of equations directly,

such as by using the Gauss elimination method. And the size of memory for storing the coefficient matrix is $O(N^2)$ as for a problem involving N degrees of freedom. Obviously, the acoustic design sensitivity analysis will take much more computing time and storage requirement than its original acoustic state analysis.

Many fast methods, such as the fast multipole methods (FMM), the fast direct solver and the adaptive cross approximation technique, have been applied to accelerate the solution of the integral equation. The fast direct solver which directly constructed a compressed factorization of the inverse of the matrix was presented by Martinsson and Rokhlin [11–13] and it is suitable for problems involving relatively ill-conditioned matrixes. The adaptive cross approximation technique pioneered by Bebendorf and Rjasanow generates blockwise low-rank approximants from the BEM matrices and is a well-suited method for problems with a large number of iteration steps [14,15]. While the FMM proposed by Rokhlin and Greengard [16–18] can be used to accelerate the matrix–vector products and can decrease the memory requirement to $O(N)$. So far this method has been applied to the solution of problems for Laplace [19–21], Helmholtz [22,23] and other equations [24,25]. There are actually two forms of FMM for Helmholtz equation. One is the original FMM and the other is the diagonal form FMM [26]. But both of them fail in some way outside their preferred frequency range. However, the wideband FMM formed by combining the original FMM and the diagonal form FMM can solve the problems accurately and efficiently at all frequencies [27].

On the other hand, the implementation of a single Helmholtz boundary integral equation may have the difficulty of nonuniqueness for exterior boundary-value problems. Two major methods have been proposed to tackle this problem. One is the combined Helmholtz integral equation formulation (CHIEF) [28] which can successfully conquer the difficulty by adding some additional Helmholtz integral equations in the interior domain. And it results in an overdetermined system of equation which can be solved using a least-squares technique. But it is difficult to select the optimum number and suitable positions of the interior points, especially for the high-frequency problems. Another effective alternative to overcome the nonunique solution problem is the Burton–Miller method [29] which consists of a linear combination of the conventional boundary integral equation (CBIE) and its normal derivative equation (NDBIE). The NDBIE is hypersingular when the boundary is nonsmooth, and some special treatments should be employed in its numerical evaluation. The same situation exists for the BEM sensitivity analysis.

Recently Zheng et al. [30] employed the wideband FMBEM to three dimensional acoustic design sensitivity analysis and opened the space of acoustic structure optimization for engineering problems. However, some practical problems, for instance the noise barriers standing along expressways or railways, can be simplified to two dimensional models to predict the scattering acoustic fields. Therefore, it is also of significance to develop two dimensional acoustic design sensitivity analysis, which makes it possible to observe higher frequency characters of the analyzed problem. In this work, the original FMM, diagonal form FMM and wideband FMM are applied and compared each other. Different values of parameters affecting the performance of the wideband FMM algorithm are evaluated and a set of optimal parameters are found. Furthermore, The generalized minimum residue (GMRES) method [31] is applied to accelerate the solution of the linear system of equations. It should be stressed that this work is the first application of the Wideband FMBEM to two dimensional acoustic design sensitivity analysis.

This paper is organized as follows. The BEM and FMBEM formulations in acoustic state analysis and acoustic design sensitivity analysis are introduced in Sects. 2 and 3. The wideband-FMBEM algorithm is presented in Sect. 4. In Sect. 5, numerical examples are presented to demonstrate the efficiency and validity of the proposed algorithm. Section 6 concludes the paper with further discussions.

2 BEM formulations

2.1 BEM formulations for acoustic state analysis

Consider the following Helmholtz equation governing time-harmonic acoustic wave fields:

$$\nabla^2\phi(x) + k^2\phi(x) = 0, \qquad \forall x \in \Omega, \tag{1}$$

where ϕ is the acoustic pressure, $k = \omega/c$ the wave number, ω the angular frequency, and c the wave speed in the acoustic medium Ω.

The boundary conditions can be expressed as

$$\phi(x) = \overline{\phi}(x) \qquad x \in S_\phi, \tag{2}$$

$$q(x) = \frac{\partial\phi(x)}{\partial n(x)} = i\rho\omega\overline{v}(x) \qquad x \in S_q, \tag{3}$$

$$\phi(x) = zv(x) \qquad x \in S_z, \tag{4}$$

where $n(x)$ denotes the outward unit normal vector to the boundary S at point x, i the imaginary unit, ρ the medium density, $v(x)$ the normal velocity, z the acoustic impedance. The quantities with upper bars are assumed to be known functions prescribed on the boundary.

It is necessary to introduce a condition at infinity for exterior acoustic problems. The physical requirement that all

scattered and radiated waves are outgoing should be ensured. For two dimensional problem, that is

$$\lim_{r\to\infty} r^{1/2}\left(\frac{\partial\phi}{\partial r} - ik\phi\right) = 0, \tag{5}$$

The integral formulation of the solution to the Helmholtz equation is

$$\phi(x) = \int_S G(x,y)q(y)dS(y) - \int_S F(x,y)\phi(y)dS(y), \qquad x \in \Omega, \tag{6}$$

where x is the source point, y the field point and $G(x, y)$ the Green's function. For two dimensional problem the Green's function is given by

$$G(x,y) = \frac{i}{4}H_0^{(1)}(kr), \tag{7}$$

and

$$F(x,y) = \frac{\partial G(x,y)}{\partial n(y)} = -\frac{ik}{4}H_1^{(1)}(kr)\frac{\partial r}{\partial n(y)}, \tag{8}$$

where $r = \mid y - x \mid$, $H_n^{(1)}$ denotes the first kind Hankel function of the n th order. The derivative of the integral representation (6) with respect to the outward normal at point x for $x \in \Omega$ can be expressed as

$$q(x) = \int_S G^1(x,y)q(y)dS(y) - \int_S F^1(x,y)\phi(y)dS(y), \tag{9}$$

where

$$G^1(x,y) = \frac{\partial G(x,y)}{\partial n(x)} = \frac{ik}{4}H_1^{(1)}(kr)\frac{\partial r}{\partial n(x)}, \tag{10}$$

and

$$F^1(x,y) = \frac{\partial F(x,y)}{\partial n(x)} = \frac{ik}{4r}H_1^{(1)}(kr)n_j(x)n_j(y) - \frac{ik^2}{4}H_2^{(1)}(kr)\frac{\partial r}{\partial n(x)}\frac{\partial r}{\partial n(y)}, \tag{11}$$

where n_j is the Cartesian component of $n(x)$ or $n(y)$, and $\frac{\partial r}{\partial n} = r_{,j}n_j$. Einstein's summation convention is used throughout the paper, so repeated indices imply a summation over their range.

Letting the source point x approaches the boundary S, Eqs. (6) and (9) give the following boundary integral equations:

$$c(x)\phi(x) = \int_S G(x,y)q(y)dS(y) - \int_S F(x,y)\phi(y)dS(y), \tag{12}$$

and

$$c(x)q(x) = \int_S G^1(x,y)q(y)dS(y) - \int_S F^1(x,y)\phi(y)dS(y), \tag{13}$$

where the coefficient $c(x)$ is determined by the boundary geometry at the source point x. Equations (12) and (13) are referred to as the CBIE and NDBIE formulas. It is well-known that the CBIE or NDBIE for exterior boundary-value problems may have difficulty of nonuniqueness. However, the linear combination of them can yield unique solutions for all frequencies, if the coupling constant of the two equations is a complex [32].

If the boundary is nonsmooth, Eq. (12) is a strongly singular boundary integral equation and Eq. (13) is a hypersingular boundary integral equation. Such integrals usually need special treatments but they can be evaluated explicitly and directly with the Cauchy principal value and the Hadamard finite part integral method respectively by using piecewise constant discretization (or called zero order element) [33,34]. Thus, in such piecewise constant discretization, as for 2D problems, the CBIE and NDBIE formulas can be rewritten as

$$\frac{1}{2}\phi(x) - C_1q(x) = \int_{S\setminus S_x} G(x,y)q(y)dS(y) - \int_{S\setminus S_x} F(x,y)\phi(y)dS(y), \tag{14}$$

and

$$\frac{1}{2}q(x) - C_2\phi(x) = \int_{S\setminus S_x} G^1(x,y)q(y)dS(y) - \int_{S\setminus S_x} F^1(x,y)\phi(y)dS(y), \tag{15}$$

where

$$C_1 = \frac{i}{4} \lim_{\varepsilon \to 0} \int_{\Gamma_\varepsilon} H_0^{(1)}(kr) dS(y), \tag{16}$$

and

$$C_2 = \lim_{\varepsilon \to 0} \left[\int_{\Gamma_\varepsilon} \frac{ik}{4r} H_1^{(1)}(kr) dS(y) - \frac{1}{\pi \varepsilon} \right]. \tag{17}$$

$S \setminus S_x$ denotes the boundary S except S_x, S_x is the element containing the source point x. S_ε denotes a semi-circle with a radius ε centred at x and Γ_ε denotes $S_x \setminus S_\varepsilon$, as shown in Fig. 1. L is the length of the element in which point x locates. By eliminating the singular parts in functions $H_0^{(1)}(kr)$ and $H_1^{(1)}(kr)/(kr)$, the coefficients C_1 and C_2 can be expressed respectively by the following two formulations:

$$C_1 = -\frac{L}{2\pi} \left[\ln\left(\frac{kL}{2}\right) - 1 \right] + \frac{i}{4} \lim_{\varepsilon \to 0} \int_{\Gamma_\varepsilon} \left[H_0^{(1)}(kr) - \frac{2i}{\pi} \ln(kr) \right] dS(y), \tag{18}$$

and

$$C_2 = \frac{ik^2}{4} \lim_{\varepsilon \to 0} \int_{\Gamma_\varepsilon} \left[\frac{H_1^{(1)}(kr)}{kr} + \frac{2i}{\pi k^2 r^2} - \frac{i}{\pi} \ln(kr) \right] dS(y) - \frac{k^2 L}{4\pi} \left[\ln\left(\frac{kL}{2}\right) + \frac{8}{k^2 L^2} - 1 \right], \tag{19}$$

where the non-singular integrals can be calculated by using Gauss quadrature.

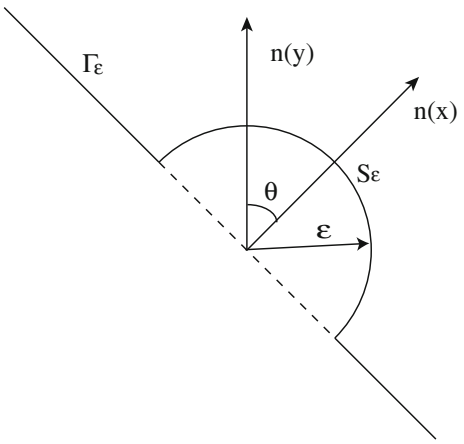

Fig. 1 An infinitesimal hemicircle attached to the zero order element S_x

The linear combination of Eqs. (14) and (15) can be expressed as

$$\int_{S \setminus S_x} [G(x, y)q(y) - F(x, y)\phi(y)] dS(y) + \alpha \int_{S \setminus S_x} \left[G^1(x, y)q(y) - F^1(x, y)\phi(y) \right] dS(y) = \left(\frac{1}{2} + \alpha C_2 \right) \phi(x) - \left(C_1 - \frac{\alpha}{2} \right) q(x), \tag{20}$$

where α can be chosen as i/k for $k \geqslant 1$, but i for $k < 1$ [35].

If the boundary S is divided into N elements (e.g. using piecewise constant discretization in this study). Then, after collecting the equations for all collocation points (nodes) located at the centre of each element and expressing them in matrix forms, one can obtain the following system of linear algebraic equations:

$$[H]\{\phi\} = [G]\{q\}. \tag{21}$$

Moving all the unknown terms of Eq. (21) to the left-hand side and all the known terms to the right-hand side by considering the boundary conditions (e.g. for Neumann type problems, the pressure ϕ is unknown and the normal derivative q is specified), one finally obtain the following system of linear equations:

$$[A]\{x\} = \{b\}, \tag{22}$$

where $[A]$ is the coefficient matrix, $\{x\}$ the vector of unknown boundary values at the nodes, $\{b\}$ the known vector. All the unknown boundary state values can be obtained after Eq. (22) is solved. Finally, one can calculate the sound pressure ϕ at any interior point by using Eq. (6).

2.2 BEM formulations for acoustic design sensitivity analysis

By differentiating Eqs. (6) and (9) with respect to an arbitrary design variable, one can obtain the following formulations for acoustic design sensitivity analysis:

$$\dot{\phi}(x) = \int_S [\dot{G}(x, y)q(y) - \dot{F}(x, y)\phi(y)] dS(y) + \int_S [G(x, y)\dot{q}(y) - F(x, y)\dot{\phi}(y)] dS(y) + \int_S [G(x, y)q(y) - F(x, y)\phi(y)] d\dot{S}(y), \tag{23}$$

and

$$\dot{q}(x) = \int_S [\dot{G}^1(x,y)q(y) - \dot{F}^1(x,y)\phi(y)]dS(y) + \int_S [G^1(x,y)\dot{q}(y) - F^1(x,y)\dot{\phi}(y)]dS(y) + \int_S [G^1(x,y)q(y) - F^1(x,y)\phi(y)]d\dot{S}(y), \quad (24)$$

where the upper dot $\dot{(\,)}$ denotes the differentiation with respect to the design variable, and $\dot{F}(x,y)$, $\dot{G}(x,y)$, $\dot{F}^1(x,y)$, $\dot{G}^1(x,y)$, $d\dot{S}(y)$ can be expressed in the form of the coordinate sensitivity, as follows:

$$\dot{G}(x,y) = -\frac{ik}{4}H_1^{(1)}(kr)\dot{r}, \quad (25)$$

$$\dot{F}(x,y) = -\frac{ik}{4}H_1^{(1)}(kr)\left[\frac{(\dot{y}_j - \dot{x}_j)n_j(y)}{r} + r_{,j}\dot{n}_j(y)\right] + \frac{ik^2}{4}H_2^{(1)}(kr)\dot{r}r_{,j}n_j(y), \quad (26)$$

$$\dot{G}^1(x,y) = \frac{ik}{4}H_1^{(1)}(kr)\left[\frac{(\dot{y}_j - \dot{x}_j)n_j(x)}{r} + r_{,j}\dot{n}_j(x)\right] - \frac{ik^2}{4}H_2^{(1)}(kr)\dot{r}r_{,j}n_j(x), \quad (27)$$

and

$$\begin{aligned}\dot{F}^1(x,y) =& \frac{ik}{4r}H_1^{(1)}(kr)\dot{\overline{n_j(x)n_j(y)}} + \frac{ik^3}{4}H_3^{(1)}(kr)\dot{r}r_{,j}n_j(x)r_{,l}n_l(y) \\ &- \frac{ik^2}{4}H_2^{(1)}(kr)\frac{n_j(x)n_j(y)\dot{r}}{r} - \frac{ik^2}{4}H_2^{(1)}(kr)r_{,j}n_j(x)\dot{\overline{r_{,l}n_l(y)}} \\ &- \frac{ik^2}{4}H_2^{(1)}(kr)\dot{\overline{r_{,j}n_j(x)}}r_{,l}n_l(y) - \frac{ik^2}{4}H_2^{(1)}(kr)\frac{2\dot{r}r_{,j}n_j(x)r_{,l}n_l(y)}{r}, \end{aligned} \quad (28)$$

where

$$\dot{r} = r_{,j}(\dot{y}_j - \dot{x}_j), \quad (29)$$

and

$$\dot{\overline{r_{,l}n_l(y)}} = \frac{(\dot{y}_l - \dot{x}_l)n_l(y)}{r} - \frac{\dot{r}r_{,l}n_l(y)}{r} + r_{,l}\dot{n}_l(y). \quad (30)$$

$\dot{x}_j$ and $\dot{y}_j$ will be evaluated when the boundary of the analyzed domain is fully parameterized with the shape design variable. According to [36], $\dot{n}_l(y)$ and $d\dot{S}(y)$ can be written as

$$\dot{n}_l(y) = -\dot{y}_{j,l}n_j(y) + \dot{y}_{j,m}n_j(y)n_m(y)n_l(y), \quad (31)$$

and

$$d\dot{S}(y) = [\dot{y}_{l,l} - \dot{y}_{l,j}n_l(y)n_j(y)]dS(y), \quad (32)$$

where an index after a comma denotes the partial derivative with respect to the coordinate component and $\dot{y}_{j,m} = \partial\dot{y}_j/\partial y_m$.

If point x approaches the boundary S in Eqs. (23) and (24), one can obtain the following formulations for acoustic design sensitivity analysis:

$$\begin{aligned}c(x)\dot{\phi}(x) =& \int_S [\dot{G}(x,y)q(y) - \dot{F}(x,y)\phi(y)]dS(y) + \int_S [G(x,y)\dot{q}(y) - F(x,y)\dot{\phi}(y)]dS(y) \\ &+ \int_S [G(x,y)q(y) - F(x,y)\phi(y)]d\dot{S}(y), \end{aligned} \quad (33)$$

and

$$\begin{aligned}c(x)\dot{q}(x) =& \int_S [\dot{G}^1(x,y)q(y) - \dot{F}^1(x,y)\phi(y)]dS(y) + \int_S [G^1(x,y)\dot{q}(y) - F^1(x,y)\dot{\phi}(y)]dS(y) \\ &+ \int_S [G^1(x,y)q(y) - F^1(x,y)\phi(y)]d\dot{S}(y). \end{aligned} \quad (34)$$

Obviously, the singularities in Eqs. (33) and (34) are the same as those in Eqs. (12) and (13), and the related integrals can be evaluated explicitly in terms of the Cauchy principal value and the Hadamard finite part integral method by using the piecewise constant discretization. For this discretization, the details of the evaluation process are given in Appendix A. Finally, the non-singular boundary integral formulations of Eqs. (33) and (34) can be written as

$$\begin{aligned}\frac{1}{2}\dot{\phi}(x) =& A_1 + \int_{S\setminus S_x} [\dot{G}(x,y)q(y) - \dot{F}(x,y)\phi(y)]dS(y) + \int_{S\setminus S_x} [G(x,y)\dot{q}(y) - F(x,y)\dot{\phi}(y)]dS(y) \\ &+ \int_{S\setminus S_x} [G(x,y)q(y) - F(x,y)\phi(y)]d\dot{S}(y), \end{aligned} \quad (35)$$

and

$$\frac{1}{2}\dot{q}(x) = B_1 + \int_{S\setminus S_x} [\dot{G}^1(x,y)q(y) - \dot{F}^1(x,y)\phi(y)]dS(y) + \int_{S\setminus S_x} [G^1(x,y)\dot{q}(y) - F^1(x,y)\dot{\phi}(y)]dS(y) + \int_{S\setminus S_x} [G^1(x,y)q(y) - F^1(x,y)\phi(y)]d\dot{S}(y), \tag{36}$$

where

$$A_1 = -\frac{ik}{4}\lim_{\varepsilon\to 0}\int_{\Gamma_\varepsilon} H_1^{(1)}(kr)\dot{r}dS(y)q(x) + C_1\dot{q}(x) + C_1 q(x)[\dot{x}_{l,l} - \dot{x}_{l,j}n_l(x)n_j(x)], \tag{37}$$

and

$$B_1 = -\frac{ik^2}{4}\lim_{\varepsilon\to 0}\int_{\Gamma_\varepsilon}\left[H_2^{(1)}(kr) + \frac{4i}{\pi k^2 r^2}\right]dS(y)r_{,l}r_{,j}\dot{x}_{l,j}\phi(x) + \left(\frac{4}{\pi L} + C_2\right)r_{,l}r_{,j}\dot{x}_{l,j}\phi(x) + C_2\dot{\phi}(x). \tag{38}$$

In fact, one can also obtain Eqs. (35) and (36) by differentiating Eqs. (14) and (15) with respect to the design variable directly, and the details of the deduction process are given in Appendix B.

For exterior boundary-value problems, Eq. (35) or (36) may give rise to the difficulty of the nonuniqueness. However, the linear combination of them provides unique solutions for all frequencies and it can be expressed as

$$\frac{1}{2}\dot{\phi}(x) = \int_{S\setminus S_x} [\dot{G}(x,y)q(y) - \dot{F}(x,y)\phi(y)]dS(y) + \int_{S\setminus S_x} [G(x,y)\dot{q}(y) - F(x,y)\dot{\phi}(y)]dS(y) + \int_{S\setminus S_x} [G(x,y)q(y) - F(x,y)\phi(y)]d\dot{S}(y) + \alpha\int_{S\setminus S_x} [\dot{G}^1(x,y)q(y) - \dot{F}^1(x,y)\phi(y)]dS(y) + \alpha\int_{S\setminus S_x} [G^1(x,y)\dot{q}(y) - F^1(x,y)\dot{\phi}(y)]dS(y) + \alpha\int_{S\setminus S_x} [G^1(x,y)q(y) - F^1(x,y)\phi(y)]d\dot{S}(y) - \frac{\alpha}{2}\dot{q}(x) + A_1 + \alpha B_1. \tag{39}$$

After obtaining all the unknown boundary state values by solving Eq. (22) and subsequently substituting all the boundary state values into the discretized form of Eq. (39), one can obtain the following equation:

$$[A]\{y\} = \{c\}, \tag{40}$$

where $[A]$ is the same matrix as that in Eq. (22), $\{y\}$ the vector of unknown boundary sensitivity values at the nodes, $\{c\}$ the known vector. All the unknown boundary sensitivity values can be obtained after Eq. (40) is solved. Finally, one can calculate the sensitivity value $\dot{\phi}$ at any interior point by using Eq. (23).

3 FMM formulations

In this section, the FMM approach is introduced to accelerate the matrix-vector product and the iterative solver GMRES is used to solve Eqs. (22) and (40). First, the fundamentals of the original FMM (low-frequency method) are presented. It is well-known that the original FMM is inefficient for high frequency problems, so the diagonal form (high-frequency method) is introduced to overcome this difficulty. But the diagonal form has instability problem for the solution of low frequency Helmholtz equations. Following the work of Zheng et al. [30], a wideband FMM for two dimensional acoustic design sensitivity analysis is constructed to overcome the above problems.

3.1 Original FMM formulations

3.1.1 Original FMM formulations for acoustic state analysis

With Graf's addition theorem, the Green's function (7) can be expanded into the following series:

$$G(x,y) = \frac{i}{4}\sum_{n=-\infty}^{+\infty} O_n(\overrightarrow{y_c x})I_{-n}(\overrightarrow{y_c y}), \tag{41}$$

where y_c is an expansion point near y, the functions O_n and I_n are defined by

$$O_n(\mathbf{x}) = i^n H_n^{(1)}(kr)e^{in\theta}, \tag{42}$$

and

$$I_n(\mathbf{x}) = (-i)^n J_n(kr)e^{in\theta}, \tag{43}$$

where J_n denotes the n th order Bessel function, (r, θ) indicates the polar coordinate of vector $\mathbf{x}$.

S_0 stands for a subset of the boundary S, which is far away from the source point x. First, the integrals in Eq. (20) can be reformulated by

$$A_2 = \int_{S_0} [G(x, y)q(y) - F(x, y)\phi(y)]dS(y), \tag{44}$$

and

$$B_2 = \int_{S_0} [G^1(x, y)q(y) - F^1(x, y)\phi(y)]dS(y). \tag{45}$$

By substituting Eq. (41) into Eqs. (44) and (45), we can obtain the following formulas:

$$A_2 = \sum_{n=-\infty}^{+\infty} O_n(\overrightarrow{y_c x})M_n(y_c), \tag{46}$$

and

$$B_2 = \sum_{n=-\infty}^{+\infty} \frac{\partial O_n(\overrightarrow{y_c x})}{\partial n(x)} M_n(y_c), \tag{47}$$

where M_n is the multipole moment defined by

$$M_n(y_c) = \frac{i}{4}\int_{S_0} [I_{-n}(\overrightarrow{y_c y})q(y) - D_n(\overrightarrow{y_c y})\phi(y)]dS(y), \tag{48}$$

where y_c is located close to S_0 and $D_n(\overrightarrow{y_c y})$ is given by

$$D_n(\overrightarrow{y_c y}) = \frac{\partial I_{-n}(\overrightarrow{y_c y})}{\partial n(y)}. \tag{49}$$

The M2M, M2L, L2L translation formulas are given by

$$M_n(y_c^1) = \sum_{m=-\infty}^{+\infty} I_{-n+m}(\overrightarrow{y_c^1 y_c})M_m(y_c), \tag{50}$$

$$L_n(x_l) = \sum_{m=-\infty}^{+\infty} (-1)^n O_{n-m}(\overrightarrow{y_c^1 x_l})M_{-m}(y_c^1), \tag{51}$$

and

$$L_n(x_l^1) = \sum_{m=-\infty}^{+\infty} I_{n-m}(\overrightarrow{x_l^1 x_l})L_m(x_l), \tag{52}$$

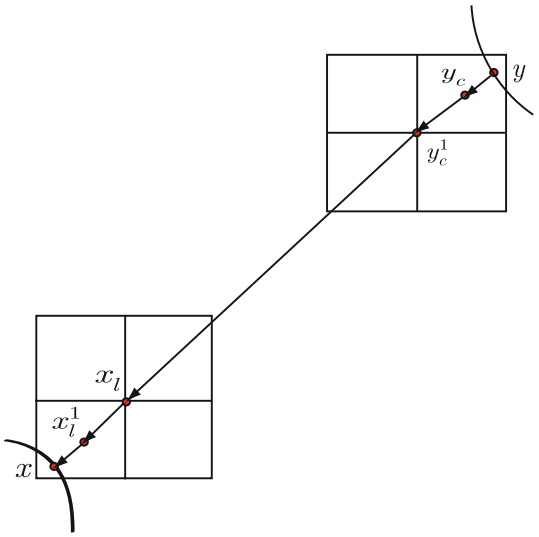

Fig. 2 Multipole expansion points and the boundary nodes

where y_c^1 is located close to S_0, x_l and x_l^1 close to x, as shown in Fig. 2.

To the end, one can obtain the following formulations:

$$A_2 = \sum_{n=-\infty}^{+\infty} I_{-n}(\overrightarrow{x_l^1 x})L_n(x_l^1), \tag{53}$$

and

$$B_2 = \sum_{n=-\infty}^{+\infty} D_n(\overrightarrow{x_l^1 x})L_n(x_l^1). \tag{54}$$

3.1.2 Original FMM formulations for acoustic design sensitivity analysis

By differentiating Eq. (41) with respect to the design variable, one can obtain the following expression:

$$\begin{aligned}\dot{G}(x, y) =& \frac{i}{4}\sum_{n=-\infty}^{+\infty} \dot{O}_n(\overrightarrow{y_c x})I_{-n}(\overrightarrow{y_c y}) \\ &+ \frac{i}{4}\sum_{n=-\infty}^{+\infty} O_n(\overrightarrow{y_c x})\dot{I}_{-n}(\overrightarrow{y_c y}),\end{aligned} \tag{55}$$

and then, one can obtain

$$\begin{aligned}\dot{F}(x, y) =& \frac{i}{4}\sum_{n=-\infty}^{+\infty} \dot{O}_n(\overrightarrow{y_c x})D_n(\overrightarrow{y_c y}) \\ &+ \frac{i}{4}\sum_{n=-\infty}^{+\infty} O_n(\overrightarrow{y_c x})\dot{D}_n(\overrightarrow{y_c y}),\end{aligned} \tag{56}$$

where $\dot{I}_{-n}(\overrightarrow{y_c y})$ and $\dot{D}_n(\overrightarrow{y_c y})$ are defined by

$$\dot{I}_{-n}(\overrightarrow{y_c y}) = (-i)^n \left[n J_n(kr) \left(\frac{\dot{r}}{r} - i\dot{\theta} \right) - J_{n+1}(kr) k\dot{r} \right] e^{-in\theta}, \tag{57}$$

and

$$\begin{aligned} \dot{D}_n(\overrightarrow{y_c y}) =& (-i)^n e^{-i(\beta+n\theta)} \\ & \times \left\{ J_{n-1}(kr) \left[\frac{\dot{r}(n-1)}{r} - i(\dot{\beta} + n\dot{\theta}) \right] - k\dot{r} J_n(kr) \right\} \\ & - (-i)^n e^{i(\beta-n\theta)} \\ & \times \left\{ J_{n+1}(kr) \left[\frac{\dot{r}(n+1)}{r} + i(\dot{\beta} - n\dot{\theta}) \right] - k\dot{r} J_{n+2}(kr) \right\}, \end{aligned} \tag{58}$$

where β denotes the angle between the vector from y_c to y and the outward normal at point y.

First, the integrals in Eq. (39) can be reformulated by:

$$\begin{aligned} D_1 =& \int_{S_0} [\dot{G}(x,y) q(y) - \dot{F}(x,y) \phi(y)] dS(y) \\ & + \alpha \int_{S_0} [\dot{G}^1(x,y) q(y) - \dot{F}^1(x,y) \phi(y)] dS(y), \end{aligned} \tag{59}$$

$$\begin{aligned} D_2 =& \int_{S_0} [G(x,y) \dot{q}(y) - F(x,y) \dot{\phi}(y)] dS(y) \\ & + \alpha \int_{S_0} [G^1(x,y) \dot{q}(y) - F^1(x,y) \dot{\phi}(y)] dS(y), \end{aligned} \tag{60}$$

and

$$\begin{aligned} D_3 =& \int_{S_0} [G(x,y) q(y) - F(x,y) \phi(y)] d\dot{S}(y) \\ & + \alpha \int_{S_0} [G^1(x,y) q(y) - F^1(x,y) \phi(y)] d\dot{S}(y). \end{aligned} \tag{61}$$

By substituting Eqs. (41), (55) and (56) into Eqs. (59)–(61), one can obtain the following formulations:

$$\begin{aligned} D_1 =& \sum_{n=-\infty}^{\infty} \left[\dot{O}_n(\overrightarrow{y_c x}) + \alpha \overline{\frac{\partial O_n(\overrightarrow{y_c x})}{\partial n(x)}} \right] M_n(y_c) \\ & + \sum_{n=-\infty}^{\infty} \left[O_n(\overrightarrow{y_c x}) + \alpha \frac{\partial O_n(\overrightarrow{y_c x})}{\partial n(x)} \right] M_n^1(y_c), \end{aligned} \tag{62}$$

$$D_2 = \sum_{n=-\infty}^{\infty} \left[O_n(\overrightarrow{y_c x}) + \alpha \frac{\partial O_n(\overrightarrow{y_c x})}{\partial n(x)} \right] M_n^2(y_c), \tag{63}$$

and

$$D_3 = \sum_{n=-\infty}^{\infty} \left[O_n(\overrightarrow{y_c x}) + \alpha \frac{\partial O_n(\overrightarrow{y_c x})}{\partial n(x)} \right] M_n^3(y_c), \tag{64}$$

where

$$M_n^1(y_c) = \frac{i}{4} \int_{S_0} \left[\dot{I}_{-n}(\overrightarrow{y_c y}) q(y) - \dot{D}_n(\overrightarrow{y_c y}) \phi(y) \right] dS(y), \tag{65}$$

$$M_n^2(y_c) = \frac{i}{4} \int_{S_0} \left[I_{-n}(\overrightarrow{y_c y}) \dot{q}(y) - D_n(\overrightarrow{y_c y}) \dot{\phi}(y) \right] dS(y), \tag{66}$$

and

$$M_n^3(y_c) = \frac{i}{4} \int_{S_0} \left[I_{-n}(\overrightarrow{y_c y}) q(y) - D_n(\overrightarrow{y_c y}) \phi(y) \right] d\dot{S}(y). \tag{67}$$

Actually, the M2M, M2L, L2L translation formulas for Eqs. (65)–(67) are the same as Eqs. (50)–(52). Finally D_1, D_2 and D_3 can be expressed in terms of local expansion coefficients as

$$\begin{aligned} D_1 =& \sum_{n=-\infty}^{\infty} \left[\dot{I}_{-n}(\overrightarrow{x_l x}) + \alpha \dot{D}_n(\overrightarrow{x_l x}) \right] L_n(x_l) \\ & + \sum_{n=-\infty}^{\infty} \left[I_{-n}(\overrightarrow{x_l x}) + \alpha D_n(\overrightarrow{x_l x}) \right] L_n^1(x_l), \end{aligned} \tag{68}$$

$$D_2 = \sum_{n=-\infty}^{\infty} \left[I_{-n}(\overrightarrow{x_l x}) + \alpha D_n(\overrightarrow{x_l x}) \right] L_n^2(x_l), \tag{69}$$

and

$$D_3 = \sum_{n=-\infty}^{\infty} \left[I_{-n}(\overrightarrow{x_l x}) + \alpha D_n(\overrightarrow{x_l x}) \right] L_n^3(x_l). \tag{70}$$

3.2 Diagonal formulations

3.2.1 Diagonal formulations for acoustic state analysis

The plane wave expansion of the Green's function (7) can be written as

$$G(x,y) = \frac{i}{8\pi} \oint e^{ik\hat{k}\cdot\overrightarrow{x_l x}} T(\theta, \overrightarrow{y_c x_l}) e^{-ik\hat{k}\cdot\overrightarrow{y_c y}} d\theta, \tag{71}$$

where

$$\hat{k}(\theta) = (\cos\theta, \sin\theta), \tag{72}$$

and

$$T(\theta, \overrightarrow{y_c x_l}) = \sum_{n=-\infty}^{\infty} e^{-in\theta} O_n(\overrightarrow{y_c x_l}). \tag{73}$$

By substituting Eq. (71) into (44), one have

$$A_2 = \frac{i}{8\pi} \oint e^{ik\hat{k}\cdot\overrightarrow{x_l x}} T(\theta, \overrightarrow{y_c x_l}) B(\theta, y_c) d\theta, \tag{74}$$

where $B(\theta, y_c)$ is the high-frequency moments defined by

$$B(\theta, y_c) = \int_{S_0} \left[e^{-ik\hat{k}\cdot\overrightarrow{y_c y}} q(y) - E(\overrightarrow{y_c y}) \phi(y) \right] dS(y), \tag{75}$$

and

$$E(\overrightarrow{y_c y}) = \frac{\partial e^{-ik\hat{k}\cdot\overrightarrow{y_c y}}}{\partial n(y)}. \tag{76}$$

The B2B, B2H and H2H translation formulas are given by

$$B(\theta, y_c^1) = e^{-ik\hat{k}\cdot\overrightarrow{y_c^1 y_c}} B(\theta, y_c), \tag{77}$$

$$H(\theta, x_l) = T\left(\theta, \overrightarrow{y_c^1 x_l}\right) B(\theta, y_c^1), \tag{78}$$

and

$$H(\theta, x_l^1) = e^{ik\hat{k}\cdot\overrightarrow{x_l x_l^1}} H(\theta, x_l). \tag{79}$$

To the end, the boundary integrals can be expressed as

$$A_2 = \frac{i}{8\pi} \oint e^{ik\hat{k}\cdot\overrightarrow{x_l^1 x}} H(\theta, x_l^1) d\theta. \tag{80}$$

Similar procedure, Eq. (45) has the following form:

$$B_2 = \frac{i}{8\pi} \oint \frac{\partial e^{ik\hat{k}\cdot\overrightarrow{x_l^1 x}}}{\partial n(x)} H(\theta, x_l^1) d\theta. \tag{81}$$

3.2.2 Diagonal formulations for acoustic sensitivity analysis

By differentiating Eq. (71) with respect to the design variable, one can obtain the following expression:

$$\dot{G}(x, y) = \frac{i}{8\pi} \oint e^{ik\hat{\dot{k}}\cdot\overrightarrow{x_l x}} T\left(\theta, \overrightarrow{y_c x_l}\right) e^{-ik\hat{k}\cdot\overrightarrow{y_c y}} d\theta + \frac{i}{8\pi} \oint e^{ik\hat{k}\cdot\overrightarrow{x_l x}} T\left(\theta, \overrightarrow{y_c x_l}\right) e^{-ik\hat{\dot{k}}\cdot\overrightarrow{y_c y}} d\theta, \tag{82}$$

and then, one can obtain

$$\dot{F}(x, y) = \frac{i}{8\pi} \oint e^{ik\hat{\dot{k}}\cdot\overrightarrow{x_l x}} T\left(\theta, \overrightarrow{y_c x_l}\right) E\left(\theta, \overrightarrow{y_c y}\right) d\theta + \frac{i}{8\pi} \oint e^{ik\hat{k}\cdot\overrightarrow{x_l x}} T\left(\theta, \overrightarrow{y_c x_l}\right) \dot{E}\left(\theta, \overrightarrow{y_c y}\right) d\theta. \tag{83}$$

By substituting Eqs. (82) and (83) into Eqs. (59)–(61), one can obtain the following formulations:

$$D_1 = \frac{i}{8\pi} \oint \left[e^{ik\hat{\dot{k}}\cdot\overrightarrow{x_l x}} + \alpha \overrightarrow{\frac{\partial e^{ik\hat{k}\cdot\overrightarrow{x_l x}}}{\partial n(x)}} \right] T\left(\theta, \overrightarrow{y_c x_l}\right) B(\theta, y_c) d\theta + \frac{i}{8\pi} \oint \left[e^{ik\hat{k}\cdot\overrightarrow{x_l x}} + \alpha \frac{\partial e^{ik\hat{k}\cdot\overrightarrow{x_l x}}}{\partial n(x)} \right] T\left(\theta, \overrightarrow{y_c x_l}\right) B^1(\theta, y_c) d\theta, \tag{84}$$

$$D_2 = \frac{i}{8\pi} \oint \left[e^{ik\hat{k}\cdot\overrightarrow{x_l x}} + \alpha \frac{\partial e^{ik\hat{k}\cdot\overrightarrow{x_l x}}}{\partial n(x)} \right] T\left(\theta, \overrightarrow{y_c x_l}\right) B^2(\theta, y_c) d\theta, \tag{85}$$

and

$$D_3 = \frac{i}{8\pi} \oint \left[e^{ik\hat{k}\cdot\overrightarrow{x_l x}} + \alpha \frac{\partial e^{ik\hat{k}\cdot\overrightarrow{x_l x}}}{\partial n(x)} \right] T\left(\theta, \overrightarrow{y_c x_l}\right) B^3(\theta, y_c) d\theta, \tag{86}$$

where

$$B^1(\theta, y_c) = \int_{S_0} \left[e^{-ik\hat{\dot{k}}\cdot\overrightarrow{y_c y}} q(y) - \dot{E}\left(\theta, \overrightarrow{y_c y}\right) \phi(y) \right] dS(y), \tag{87}$$

$$B^2(\theta, y_c) = \int_{S_0} \left[e^{-ik\hat{k}\cdot\overrightarrow{y_c y}} \dot{q}(y) - E\left(\theta, \overrightarrow{y_c y}\right) \dot{\phi}(y) \right] dS(y), \tag{88}$$

and

$$B^3(\theta, y_c) = \int_{S_0} \left[e^{-ik\hat{k}\cdot\overrightarrow{y_c y}} q(y) - E\left(\theta, \overrightarrow{y_c y}\right) \phi(y) \right] d\dot{S}(y). \tag{89}$$

Actually, the B2B, B2H and H2H translation formulas for Eqs. (87)–(89) are the same as Eqs. (77)–(79). Finally

D_1, D_2 and D_3 can be expressed in terms of local expansion coefficients as

$$D_1 = \frac{i}{8\pi}\oint\left[e^{ik\hat{k}\cdot\overrightarrow{x_l x}} + \alpha\overline{\frac{\partial e^{ik\hat{k}\cdot\overrightarrow{x_l x}}}{\partial n(x)}}\right]H(\theta, x_l)d\theta + \frac{i}{8\pi}\oint\left[e^{ik\hat{k}\cdot\overrightarrow{x_l x}} + \alpha\frac{\partial e^{ik\hat{k}\cdot\overrightarrow{x_l x}}}{\partial n(x)}\right]H^1(\theta, x_l)d\theta, \tag{90}$$

$$D_2 = \frac{i}{8\pi}\oint\left[e^{ik\hat{k}\cdot\overrightarrow{x_l x}} + \alpha\frac{\partial e^{ik\hat{k}\cdot\overrightarrow{x_l x}}}{\partial n(x)}\right]H^2(\theta, x_l)d\theta, \tag{91}$$

and

$$D_3 = \frac{i}{8\pi}\oint\left[e^{ik\hat{k}\cdot\overrightarrow{x_l x}} + \alpha\frac{\partial e^{ik\hat{k}\cdot\overrightarrow{x_l x}}}{\partial n(x)}\right]H^3(\theta, x_l)d\theta. \tag{92}$$

3.3 Wideband FMM formulations

The wideband FMBEM obtained by combining the original form and the diagonal form of the FMBEM is accurate and efficient at any frequency. In the wideband FMBEM, we use the following M2B formula to convert the moments of the original form to those of the diagonal form:

$$B(\theta, y_c) = -4i\sum_{n=-\infty}^{+\infty} e^{in\theta}M_n(y_c). \tag{93}$$

The local expansion coefficients of the diagonal form can be converted to those of the original form by using the following H2L formula:

$$L_n(x_l) = \frac{i}{8\pi}(-1)^n\oint e^{in\theta}H(\theta, x_l)d\theta. \tag{94}$$

Actually, the number of terms used in the functions O, I, M and L and the number of the plane wave samples $\hat{k}$ along the unit circle have to be truncated. The number of truncation terms and the plane wave samples depends on the the size d of the cell and the wave number k. It is given in the following form in [18]:

$$p = kd + c\cdot\log(kd + \pi). \tag{95}$$

where c is a constant. Obviously, a larger c relates to a larger truncation number p and it normally leads to an improvement of accuracy but induces to a longer computing time and larger memory usage. Thus, it is a key parameter in the FMM algorithm.

4 Wideband FMM algorithm

4.1 Preparation

Firstly discretize the boundary S as usual as in the conventional BEM. Then take a square which contains S and call it a cell of level 0. This cell (the parent cell) is divided into four equal child cells of level 1. Keep dividing a cell in this way until the element number in that cell is less than a specified number, and call this childless cell a leaf cell. At any level of refinement, once an empty cell is encountered, its existence is forgotten and it is not used in the subsequent process. If two cells at level l share at least one vertex, they are said to be adjacent. If two cells at level l are not adjacent but their parent cells are adjacent at level $l-1$, they are said to be well-separated. The list of all well-separated cells of cell C forms the interaction list of C. Far cells of C consist of those cells whose parent cells are not adjacent to the parent cell of C.

4.2 Upward pass

Computation of the multipole moments. Calculate the multipole moments of each cell starting from a leaf cell and tracing the tree structure upward to level 2. For a leaf cell, the multipole moment of the low-frequency FMM is calculated by using Eq. (48) and that of the high-frequency FMM is calculated by using Eq. (75). For a non-leaf cell, by adding all the moments from its child cells after shifting the moments to the centre of their parent cell, one can obtain the multipole moment. For wave number k and the square side length d, if their product (kd) is less than a specified number, the moments of the low-frequency FMM are calculated by M2M translation , otherwise the moments of the high-frequency FMM are calculated by B2B translation. When kd is equal to the specified number, the moments of the low-frequency FMM need to be shifted to the moments of the high-frequency FMM by M2B translation. The procedure is repeated upward to level 2. The specified number is written as $2\pi\upsilon$, where υ denotes the switch parameter between high-frequency FMM and low-frequency FMM [37].

4.3 Downward pass

Computation of the local expansion coefficients. The local expansion coefficients of cell C at level l are the sum of two parts. One is obtained from all cells in the interaction list of C and the other is obtained from all the far cells of C. If kd of cell C is greater than or equal to the specified number, the local expansion coefficients are calculated by B2H and H2H. If kd of cell C is less than the specified number but that of C's parent cell is greater than or equal to the specified number,

the local expansion coefficients are calculated by M2L and H2L. Otherwise they are calculated by M2L and L2L.

4.4 Evaluation of the integrals

For a source point in a leaf cell C at level l, evaluation of the boundary integrals consists of two parts. The contributions from elements in leaf C and its adjacent cells are evaluated directly in the way as the conventional BEM. Then the contributions from all the cells in the interaction list and far cells of C are calculated by shifting the local expansion coefficients from the centre of C to the source point. If kd of cell C is less than the specified number, the above second part is evaluated by using Eqs. (68)–(70), otherwise by using Eqs. (90)–(92).

4.5 Choice of the switch parameter υ

When υ increases, more cells in the tree structure are calculated by the low frequency FMM, and the wideband algorithm obtains higher accuracy but takes more CPU time. When υ decreases, more cells in the tree structure are calculated by the high frequency FMM, and the wideband algorithm takes less CPU time but reduces the accuracy. To a limit, if υ is very small, the correct solution might not be obtained because of the instability of the high frequency FMM. So it is very important to choose a suitable υ value, which normally comes from careful numerical tests.

5 Numerical examples

5.1 Scattering from an infinite rigid cylinder

A numerical simulation of acoustic scattering from an infinite rigid cylinder with Neumann boundary condition, as shown in Fig. 3, is given to demonstrate the accuracy and efficiency of the present algorithm. The computation is done on a desktop PC with an Pentium 2.59 GHz processor and 3.24 GB memory.

In this example, we consider the acoustic scattering of a plane incident wave with unit amplitude on an infinite rigid cylinder with radius $a = 1.0$ m centred at point $(0, 0)$, and the plane incident wave is travelling along the positive x axis ($\theta = 0$). The analytical solution of the sound pressure at point (r, θ) is given as

$$\phi(r,\theta) = -\sum_{n=0}^{\infty} \varepsilon_n i^n \frac{J_n'(ka)}{H_n^{(1)\prime}(ka)} H_n^{(1)}(kr)\cos(n\theta), \qquad (96)$$

where ε_n denotes the Neumann symbols, i.e., $\varepsilon_0 = 1$; $\varepsilon_n = 2$ when n is greater than 0. $(\,)'$ stands for the differentiation with respect to ka.

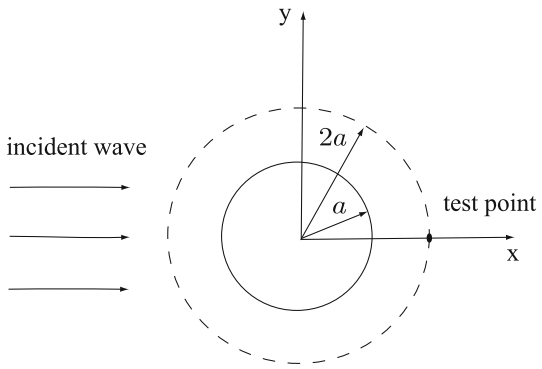

Fig. 3 Scattering from an infinite rigid cylinder with radius a

When the design variable is chosen as a, one can obtain the analytical solution of sound pressure sensitivity by differentiating Eq. (96) with respect to the design variable, as follows:

$$\frac{\partial\phi(r,\theta)}{\partial a} = -\sum_{n=0}^{\infty} \varepsilon_n i^n \left[\frac{J_n'(ka)}{H_n^{(1)\prime}(ka)}\right]' H_n^{(1)}(kr)\cos(n\theta). \qquad (97)$$

Sample internal points are evenly distributed on a circle of $r = 2a$ and the coordinates of the test point are $(2a, 0)$. The boundary of the circle is discretized with 80,000 constant elements and the maximum number of boundary elements in per leaf is set to 60. With this parameter, the number of tree levels is 10, the number of leaves is 2,196 and the number of cells is 3,829.

From Figs. 4 and 5, it can be seen that numerical results agree very well with the analytical solutions, and it demonstrates the accuracy of the algorithm. Figures 6 and 7 indicate that the sensitivity values obtained by FMBEM-CBIE cannot agree with the analytical solutions at fictitious eigenfrequencies, but FMBEM-BM (FMBEM based on Burton–Miller method) can yield excellent solutions at all frequencies. The relative error is defined as

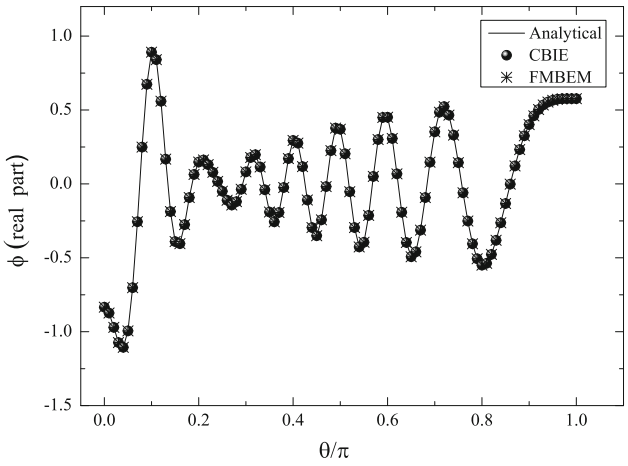

Fig. 4 Real part of pressure at points on circle $r = 2a$ with $k = 8\pi$

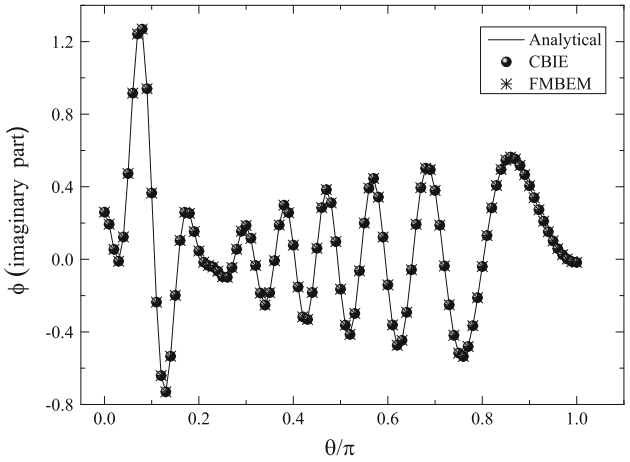

Fig. 5 Imaginary part of pressure at points on circle $r = 2a$ with $k = 8\pi$

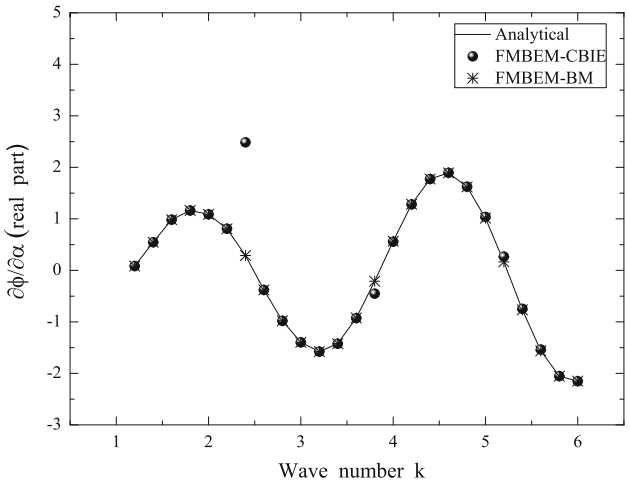

Fig. 6 Real part of pressure sensitivity at point $(2a, 0)$ with different k

$$error = \frac{|p_{numer} - p_{analy}|}{|p_{analy}|}, \tag{98}$$

where the p_{numer} denotes the numerical solution and the p_{analy} denotes the analytical solution. p can be sound pressure or its sensitivity value.

Actually, in the numerical evaluation of these boundary integral equations, truncation and numerical integration errors are the main errors. And estimates for these errors can be found in [38]. Due to the complexity of the differential equations, giving a provement of the uniform convergence of the numerical results is very hard and is not the key point for this work. However, by observing Fig. 8, it can be found that the solution converges well when refining the boundary mesh and it implicates the accuracy of the presented algorithm. The CPU time used to calculate the sensitivity values at the test point is plotted in Fig. 9, which demonstrates the

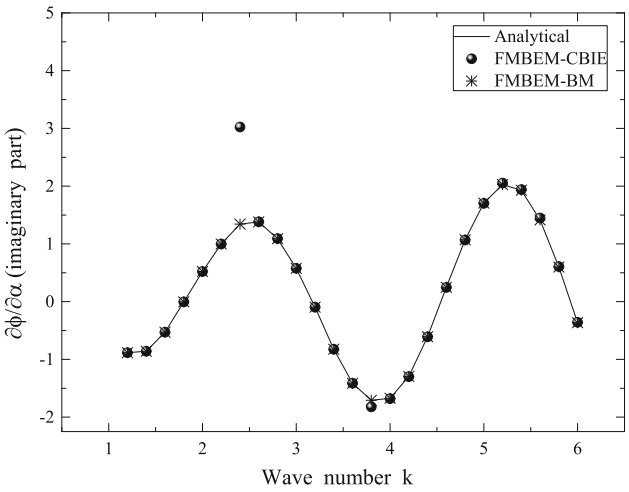

Fig. 7 Imaginary part of sensitivity at point $(2a, 0)$ with different k

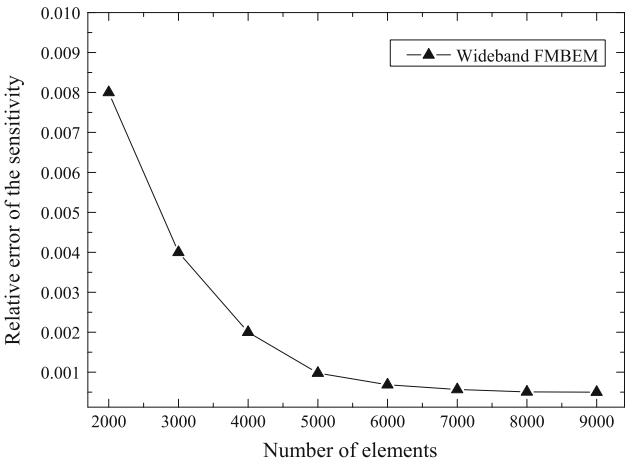

Fig. 8 Relative error of the pressure sensitivity at point $(2a, 0)$ with $k = 4\pi$

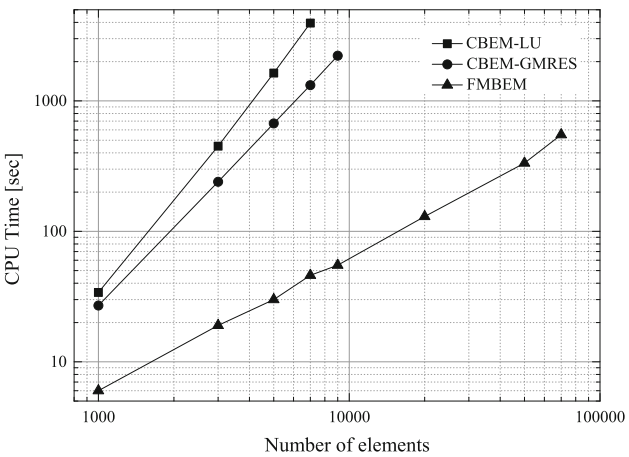

Fig. 9 CPU time used to calculate the pressure sensitivity values at point $(2a, 0)$ with $k = 4\pi$

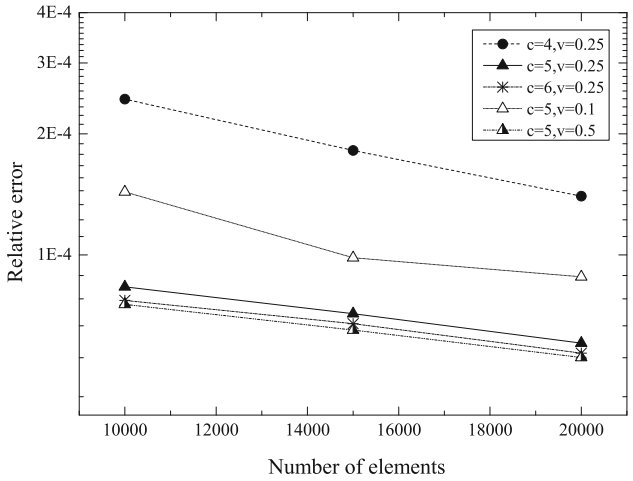

Fig. 10 Relative error at point $(2a, 0)$ with different c and v values for acoustic state analysis with $k = 4\pi$

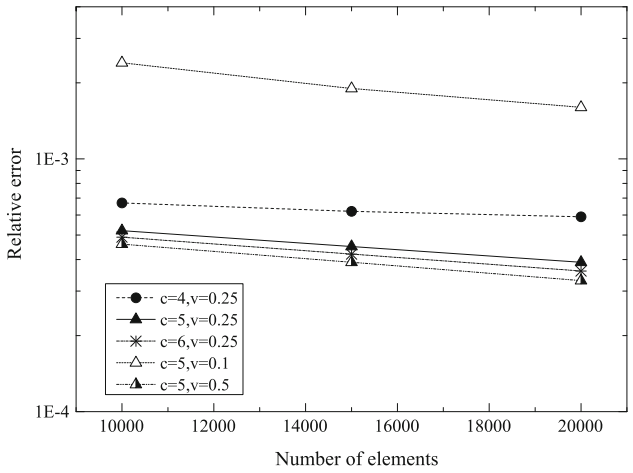

Fig. 11 Relative error at point $(2a, 0)$ with different c and v values for acoustic sensitivity analysis with $k = 4\pi$

efficiency of FMBEM for two dimensional acoustic design sensitivity analysis.

In Fig. 10 one can see the effect of constants c and v on the error of the wideband FMM solutions for acoustic state analysis, where k is set to 4π. The errors of the solutions with $c = 4$ are higher than those with larger c and the errors can further reduce with the mesh refinement. The errors with $c = 5$ and $c = 6$ for $v = 0.25$ are quite close to each other, and the errors with $v = 0.25$ and $v = 0.5$ for $c = 5$ are quite close to each other too. When the switch parameter v is chosen as 0.1, the method is still stable but the error increases. Actually the choice of parameters c and v affects the performance of the wideband FMM algorithm in terms of computing time and memory usage. Solutions with high accuracy can be obtained by increasing the value of c and v, and a high computing cost is associated with this accuracy increase. Figure 11 displays the effect of constants c and v on the errors of the wideband FMM solutions with $k = 4\pi$ for acoustic sensitivity analysis, which behaves quite similar to that in acoustic state analysis shown in Fig. 10. In view of the above results, the combination of parameters $c = 5$ and $v = 0.25$ provides a good balance between accuracy and performance, and it will be used in the following calculations.

In Table 1, 'Low', 'High' and 'Wide' denote the original FMM, the diagonal form FMM and the wideband FMM respectively. '−' means that the solution can not be obtained and it implies the numerical instability of the high-frequency FMM at low frequencies. CBEM denotes the conventional BEM method and '+' means that the solution calculated by using the CBEM method takes too long time to be get. The computing efficiency of the original FMM decreases rapidly with the ka increase. But the wideband FMM formed by combining the original FMM and the diagonal form FMM can solve this problem accurately and efficiently.

5.2 Scattering from sound barriers

Noise from expressways and railways is an important aspect of noise pollution but can be rectified by erecting barriers between the noise source and the zone to be protected. For a long straight barrier and a line source, two-dimensional model can be used to predict the acoustic field. The barrier is assumed to have infinite length and its cross section is uniform along the length. In this example, three types of barriers that are erected on a rigid, flat and sufficient large

Table 1 Computational time and relative error at the test point for CBEM and the three fast algorithms with different ka and degree of freedom

ka	DOFs	Relative error				CPU time (sec)			
		CBEM	Low	High	Wide	CBEM	Low	High	Wide
0.1	1, 500	1.27E−6	3.0E−6	-	3.0E−6	30	3	–	3
0.5	1, 500	8.1E−6	9.8E−6	5.1E−5	9.8E−6	35	4	4	4
1.0	2, 000	2.7E−6	6.1E−5	8.4E−5	6.1E−5	69	5	5	5
10	4, 000	9.3E−6	5.1E−5	6.8E−5	5.3E−5	402	27	17	18
30	6, 000	1.13e−5	6.7E−5	8.3E−5	7.9E−5	1,242	202	69	70
50	10, 000	+	2.2E−4	2.4E−4	2.4E−4	+	780	145	147

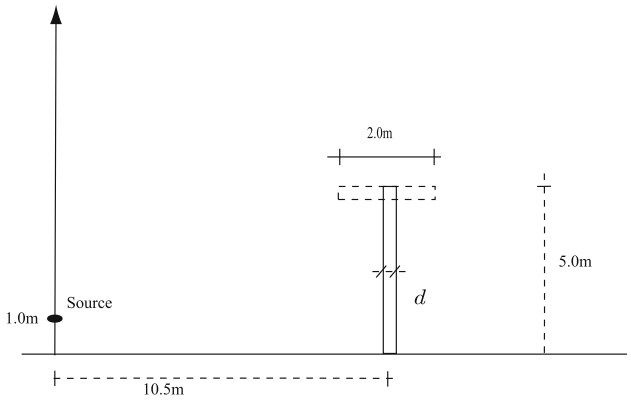

Fig. 12 Cross sections of the vertical and T-shaped barriers

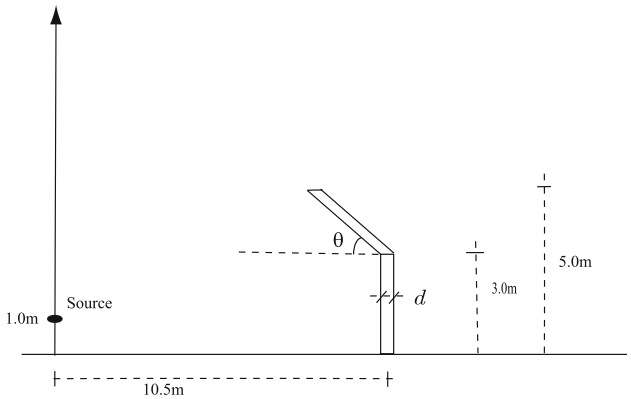

Fig. 13 Cross section of the Half-Y-shaped barrier

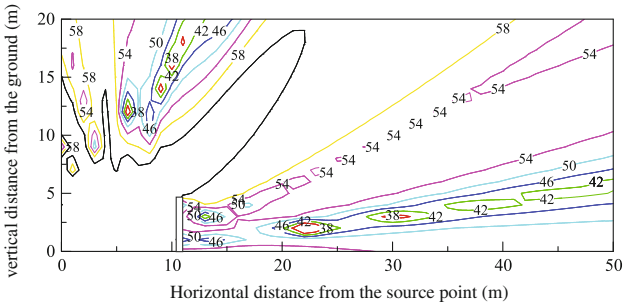

Fig. 14 Noise level distribution around a vertical barrier (db)

ground are examined. Figures 12 and 13 show their cross-section contours over a plane ground at a distance of 10.5m from a coherent homogeneous monofrequency line source situated 1.0 m above the ground. The width d of the barriers is set to 0.2 m. The source frequency is 100 Hz and all surfaces of the barriers are rigid. The vertical barrier is discretized with 120,000 zero order elements with equal length, the T-shaped barrier 138,000 zero order elements and the Half-Y-shaped barrier 124,230 zero order elements.

Figure 14 shows the sound pressure level distribution for the case of a vertical barrier, then T-shaped barrier in Fig. 15 and Half-Y-shaped barrier with angle $\theta = 40°$ in Fig. 16. The

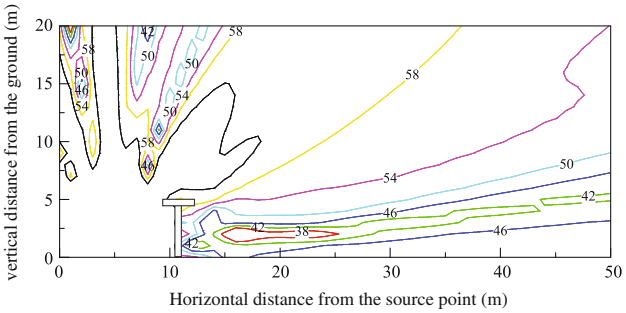

Fig. 15 Noise level distribution around a T-barrier (db)

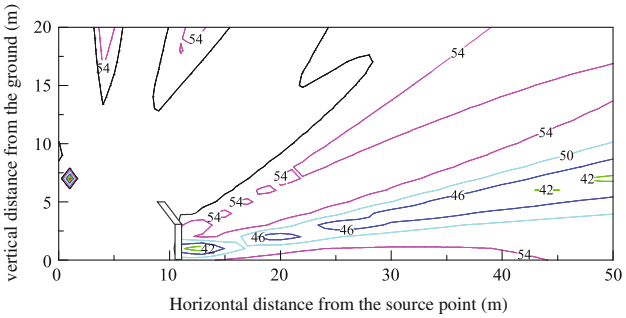

Fig. 16 Noise level distribution around a Half-Y-shaped barrier (db)

sound pressure level distribution in Fig. 14 is quite similar to that in [39], which demonstrates the correctness of the present wideband FMBEM algorithm. From the above three figures, one can find that adding substructures at the top of noise barriers has the advantage of improving the barrier performance without increasing its overall height. Figure 17 shows the distribution of the acoustic pressure level sensitivity with respect to the design variable θ as shown in Fig. 13. It can be seen that the sensitivity values within the shadow zone to be protected behind the barrier are greater than those within other areas and it implies that the noise can be controlled efficiently by choosing suitable θ value.

6 Conclusions

A wideband FMBEM has been developed for the analysis of two dimensinoal acoustic design sensitivity problems. The Burton–Miller method is used to get correct solutions at all frequencies. The strongly singular and hypersingular integrals in the sensitivity equations can be evaluated explicitly and directly with Cauchy principal value and the Hadamard finite part integral method when the zero order element is employed to discretize the boundary, where the explicite free-term expressions are given for the first time. A set of optimal parameters in the wideband FMBEM design sensitivity analysis are obtained by observing the performances of the algorithm in terms of computing time and memory usage.

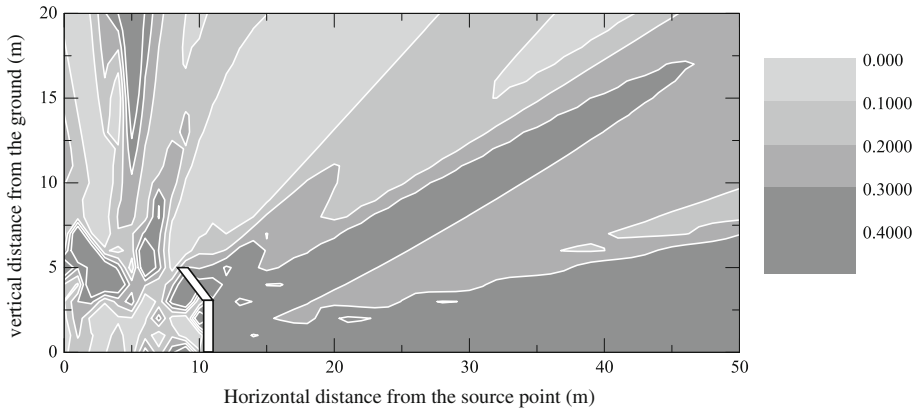

Fig. 17 Acoustic pressure level sensitivity distribution around a Half-Y-shaped barrier (db)

It can be seen that the combination of parameters $c = 5$ and $v = 0.25$ provides a good balance between accuracy and performance. Furthermore, the different performances of the low, high and wideband forms of the FMBEM are observed carefully in the 2D acoustic sensitivity analysis and the advantages of the wideband form can be easily found from the comparison of the simulation results.

Future work includes applying the acoustic design sensitivity analysis to shape optimizations and extending the method to other kinds of sensitivity problems such as potential and elastostatic problems.

Acknowledgments Financial supports from the National Natural Science Foundation of China (NSFC) under Grant No. 11172291 and China Postdoctoral Science Foundation under Grant No. 2012M510162 are acknowledged.

7 Appendix A: evaluation of the integrals on S_ϵ and Γ_ϵ

S_ϵ and Γ_ϵ are depicted in Fig. 1. The radius and shape of the semi-circle S_ϵ do not vary with respect to the design variable. First one can obtain easily the following formulations on S_ϵ:

$$n_j(x)n_j(y) = \cos\theta, \tag{99}$$

and

$$y_j - x_j = \epsilon n_j(y). \tag{100}$$

By differentiating the above two equations with respect to the design variable, one can derive the following formulations:

$$\dot{\overline{n_j(x)n_j(y)}} = 0, \tag{101}$$

and

$$\dot{\overline{y_j - x_j}} = \epsilon \dot{\overline{n_j(y)}}. \tag{102}$$

Moreover,

$$d\dot{S}(y) = 0. \tag{103}$$

By substituting the above equations into the singular integrals on boundary S_ϵ in Eqs. (33) and (34), one can obtain the following formulations:

$$\int_{S_\epsilon} F(x, y)\dot{\phi}(y)dS(y) = -\frac{1}{2}\dot{\phi}(x), \tag{104}$$

$$\int_{S_\epsilon} F^1(x, y)\dot{\phi}(y)dS(y) = -\frac{1}{\pi\epsilon}\dot{\phi}(x) - \frac{1}{4}\dot{q}(x), \tag{105}$$

and

$$\int_{S_\epsilon} G^1(x, y)\dot{q}(y)dS(y) = \frac{1}{4}\dot{q}(x). \tag{106}$$

The results of the other integrals on boundary S_ϵ in Eqs. (33) and (34) are all zero.

The element Γ_ϵ will vary with respect to the design variable and the distribution of $\dot{y}_j$ varies linearly on Γ_ϵ, one can obtain the following formulations on Γ_ϵ:

$$\dot{y}_{l,m} = \dot{x}_{l,m}, \tag{107}$$

$$\dot{y}_l - \dot{x}_l = \dot{x}_{l,j}(y_j - x_j), \tag{108}$$

and

$$d\dot{S}(y) = [\dot{y}_{l,l} - \dot{y}_{l,j}n_l(y)n_j(y)]dS(y) + r_{,l}r_{,j}\dot{x}_{l,j}\epsilon. \tag{109}$$

By substituting the above equations into the singular integrals on boundary Γ_ϵ in Eqs. (33) and (34), one can obtain the following equations:

$$\int_{\Gamma_\epsilon} \dot{G}(x,y)q(y)ds(y) = -\frac{ik}{4}\lim_{\varepsilon\to 0}\int_{\Gamma_\varepsilon} H_1^{(1)}(kr)\dot{r}dS(y)q(x), \tag{110}$$

$$\int_{\Gamma_\epsilon} G(x,y)\dot{q}(y)dS(y) = \frac{i}{4}\lim_{\varepsilon\to 0}\int_{\Gamma_\varepsilon} H_0^{(1)}(kr)dS(y)\dot{q}(x), \tag{111}$$

$$\int_{\Gamma_\epsilon} G(x,y)q(y)d\dot{S}(y) = \frac{i}{4}\lim_{\varepsilon\to 0}\int_{\Gamma_\varepsilon} H_0^{(1)}(kr)dS(y)q(x)[\dot{x}_{l,l} - \dot{x}_{l,j}n_l(x)n_j(x)], \tag{112}$$

$$\int_{\Gamma_\epsilon} F^1(x,y)\dot{\phi}(y)dS(y) = \frac{ik^2}{4}\lim_{\varepsilon\to 0}\int_{\Gamma_\varepsilon}\left[\frac{H_1^{(1)}(kr)}{kr} + \frac{2i}{\pi k^2 r^2} - \frac{i}{\pi}\ln(kr)\right]dS(y)\dot{\phi}(x) - \frac{k^2L}{4\pi}\left[\ln(\frac{kL}{2}) + \frac{8}{k^2L^2} - 1\right]\dot{\phi}(x) + \frac{1}{\pi\epsilon}\dot{\phi}(x), \tag{113}$$

$$\int_{\Gamma_\epsilon} \dot{F}^1(x,y)\phi(y)dS(y) = \left(\frac{4}{\pi L} - \frac{2}{\pi\epsilon}\right)r_{,l}r_{,j}\dot{x}_{l,j}\phi(x) - \frac{ik^2}{4}r_{,l}r_{,j}\dot{x}_{l,j}\phi(x) \cdot \lim_{\varepsilon\to 0}\int_{\Gamma_\varepsilon}\left[H_2^{(1)}(kr) + \frac{4i}{\pi k^2 r^2}\right]dS(y), \tag{114}$$

and

$$\int_{\Gamma_\epsilon} F^1(x,y)\phi(y)d\dot{S}(y) = \frac{2}{\pi\epsilon}r_{,l}r_{,j}\dot{x}_{l,j}\phi(x) + \frac{ik^2}{4}r_{,l}r_{,j}\dot{x}_{l,j}\phi(x) \cdot \lim_{\varepsilon\to 0}\int_{\Gamma_\varepsilon}\left[\frac{H_1^{(1)}(kr)}{kr} + \frac{2i}{\pi k^2 r^2} - \frac{i}{\pi}\ln(kr)\right]dS(y) - \frac{k^2L}{4\pi}\left[\ln\left(\frac{kL}{2}\right) + \frac{8}{k^2L^2} - 1\right]r_{,l}r_{,j}\dot{x}_{l,j}\phi(x). \tag{115}$$

The results of the other integrals on boundary Γ_ϵ in Eqs. (33) and (34) are all zero.

8 Appendix B: the direct differentiation wtih respect the design variable

By differentiating Eq. (14) directly with respect to the design variable, one can obtain the following equation:

$$\begin{aligned}\frac{1}{2}\dot{\phi}(x) =& \dot{C}_1 q(x) + C_1\dot{q}(x) \\ &+ \int_{S\setminus S_x}[\dot{G}(x,y)q(y) - \dot{F}(x,y)\phi(y)]dS(y) \\ &+ \int_{S\setminus S_x}[G(x,y)\dot{q}(y) - F(x,y)\dot{\phi}(y)]dS(y) \\ &+ \int_{S\setminus S_x}[G(x,y)q(y) - F(x,y)\phi(y)]d\dot{S}(y),\end{aligned} \tag{116}$$

where

$$\begin{aligned}\dot{C}_1 =& -\frac{ik}{4}\lim_{\varepsilon\to 0}\int_{\Gamma_\varepsilon} H_1^{(1)}(kr)\dot{r}dS(y) \\ &+ C_1[\dot{x}_{l,l} - \dot{x}_{l,j}n_l(x)n_j(x)].\end{aligned} \tag{117}$$

Finally, one can obtain the following equation:

$$\dot{C}_1 q(x) + C_1\dot{q}(x) = A_1. \tag{118}$$

By substituting the above equation into Eq. (116), one can obtain the same equation as Eq. (35).

By differentiating Eq. (15) directly with respect to the design variable, one can obtain the following equation:

$$\begin{aligned}\frac{1}{2}\dot{q}(x) =& \dot{C}_2\phi(x) + C_2\dot{\phi}(x) \\ &+ \int_{S\setminus S_x}[\dot{G}^1(x,y)q(y) - \dot{F}^1(x,y)\phi(y)]dS(y) \\ &+ \int_{S\setminus S_x}[G^1(x,y)\dot{q}(y) - F^1(x,y)\dot{\phi}(y)]dS(y) \\ &+ \int_{S\setminus S_x}[G^1(x,y)q(y) - F^1(x,y)\phi(y)]d\dot{S}(y),\end{aligned} \tag{119}$$

where

$$\dot{C}_2 = M_1 + M_2, \tag{120}$$

and

$$M_1 = -\frac{ik^2}{4}\lim_{\varepsilon\to 0}\int_{\Gamma_\varepsilon} H_2^{(1)}(kr)\dot{r}/rdS(y), \tag{121}$$

$$M_2 = \lim_{\varepsilon\to 0}\int_{\Gamma_\varepsilon} \frac{ik}{4r} H_1^{(1)}(kr)d\dot{S}(y). \tag{122}$$

By eliminating the singular part in function $H_2^{(1)}(kr)$, M_1 can be expressed as

$$M_1 = -\frac{ik^2}{4}\lim_{\varepsilon\to 0}\int_{\Gamma_\varepsilon}\left[H_2^{(1)}(kr)+\frac{4i}{\pi k^2 r^2}\right]\dot{r}/r dS(y) - \lim_{\varepsilon\to 0}\int_{\Gamma_\varepsilon}\frac{1}{\pi r^2}\dot{r}/r dS(y). \tag{123}$$

From Eqs. (29) and (108), one can derived the following equation on Γ_ε:

$$\dot{r}/r = r_{,l}r_{,j}\dot{x}_{l,j} = \dot{y}_{l,l} - \dot{y}_{l,j}n_l(y)n_j(y), \tag{124}$$

and $\dot{r}/r$ does not vary with respect to the design variable for the piecewise constant discretization. By substituting this equation into Eq. (123), one can obtain

$$M_1 = -\frac{ik^2}{4}\lim_{\varepsilon\to 0}\int_{\Gamma_\varepsilon}\left[H_2^{(1)}(kr)+\frac{4i}{\pi k^2 r^2}\right]dS(y)r_{,l}r_{,j}\dot{x}_{l,j} + \left(\frac{4}{\pi L}-\frac{2}{\pi\varepsilon}\right)r_{,l}r_{,j}\dot{x}_{l,j}. \tag{125}$$

By substituting Eq. (109) into Eq. (122), M_2 can be expressed as

$$M_2 = \lim_{\varepsilon\to 0}\int_{\Gamma_\varepsilon}\frac{ik}{4r}H_1^{(1)}(kr)dS(y)r_{,l}r_{,j}\dot{x}_{l,j} + \frac{1}{\pi\varepsilon}r_{,l}r_{,j}\dot{x}_{l,j}. \tag{126}$$

By substituting Eq. (17) into the above equation, one can obtain

$$M_2 = C_2 r_{,l}r_{,j}\dot{x}_{l,j} + \frac{2}{\pi\varepsilon}r_{,l}r_{,j}\dot{x}_{l,j}. \tag{127}$$

By substituting Eqs. (125) and (127) into Eq. (120), $\dot{C}_2$can be expressed as

$$\dot{C}_2 = -\frac{ik^2}{4}\lim_{\varepsilon\to 0}\int_{\Gamma_\varepsilon}\left[H_2^{(1)}(kr)+\frac{4i}{\pi k^2 r^2}\right]dS(y)r_{,l}r_{,j}\dot{x}_{l,j} + \left(\frac{4}{\pi L}+C_2\right)r_{,l}r_{,j}\dot{x}_{l,j}. \tag{128}$$

Finally, one can obtain the following equation:

$$\dot{C}_2\phi(x) + C_2\dot{\phi}(x) = B_1. \tag{129}$$

By substituting the above equation into Eq. (119), one can obtain the same equation as Eq. (36).

References

1. Gates AA, Accorsi ML (1993) Automatic shape optimization of three-dimensional shell structures with large shape changes. Comput Struct 49:167–178
2. Scarpa F (2000) Parametric sensitivity analysis of coupled acoustic-structural systems. J Vib Acoust 122:109–115
3. Sommerfeld A (1949) Partial differential equations in physics. Academic Press Inc, New York
4. Engleder S, Steinbach O (2008) Stabilized boundary element methods for exterior Helmholtz problems. Numerische Mathematik 110:145–160
5. Demkowicz L, Karafiat A, Oden JT (1991) Solution of elastic scattering problems in linear acoustic using hp boundary element method. Comput Methods Appl Mech Eng 101:251–282
6. Smith DC, Bernhard RJ (1992) Computation of acoustic shape design sensitivity using a boundary element method. J Vib Acoust 114:127–132
7. Matsumoto T, Tanaka M, Miyagawa M, Ishii N (1993) Optimum design of cooling lines in injection moulds by using boundary element design sensitivity analysis. Finite Elem Anal Des 14:177–185
8. Matsumoto T, Tanaka M, Yamada Y (1995) Design sensitivity analysis of steady-state acoustic problems using boundary integral equation formulation. JSME Int J C 38:9–16
9. Koo BU, Ih JG, Lee BC (1998) Acoustic shape sensitivity analysis using the boundary integral equation. J Acoust Soc Am 104:2851–2860
10. Kane JH, Mao S, Everstine GC (1991) A boundary element formulation for acoustic sensitivity analysis. J Acoust Soc Am 90:561–573
11. Martinsson PG, Rokhlin V (2004) A fast direct solver for boundary integral equations in two dimensions. J Comput Phys 205:1–23
12. Martinsson PG, Rokhlin V (2007) A fast direct solver for scattering problems involving elongated structures. J Comput Phys 221:288–302
13. Martinsson PG (2009) A fast direct solver for a class of elliptic partial differential equations. J Sci Comput 38(3):316–330
14. Bebendorf M, Rjasanow S (2003) Adaptive low-rank approximation of collocation matrices. Computing 70:1–24
15. Rjasanow S, Steinbach O (2007) The fast solution of boundary integral equations. Springer, Boston
16. Rokhlin V (1990) Rapid solution of integral equations of scattering theory in two dimensions. J Comput Phys 86:414–439
17. Greengard L, Rokhlin V (1987) A fast algorithm for particle simulations. J Comput Phys 73:325–348
18. Coifman R, Rokhlin V, Wandzura S (1993) The fast multipole method for the wave equation: a pedestrian prescriptions. Antennas Propag Mag IEEE 35(3):7–12
19. Liu YJ, Nishimura N, Yao ZH (2005) A fast multipole accelerated method of fundamental solutions for potential problems. Eng Anal Boundary Elem 29:1016–1024
20. Rokhlin V (1985) Rapid solution of integral equations of calssical potential theory. J Comput Phys 60:187–207
21. Liu YJ, Nishimura N (2006) The fast multipole boundary element method for potential problems. Eng Anal Boundary Elem 30:371–381
22. Shen L, Liu YJ (2007) An adaptive fast multipole boundary element method for three-dimensional acoustic wave problems based on the Burton–Miller formulations. Comput Mech 40:461–472

23. Li SD, Huang QB (2011) A new fast multipole boundary element method for two dimensional acoustic problems. Comput Methods Appl Mech Eng 200:1333–1340
24. Yoshida K, Nishimura N, Kobayashi S (2001) Application of new fast multipole boundary integral equation method to crack problems in 3D. Eng Anal Boundary Elem 25:239–247
25. Nishimura N (2002) Fast multipole accelerated boundary integral equation methods. Appl Mech Rev 55:299–324
26. Lu CC, Chew WC (1993) Fast algorithm for solving hybrid integral equations. IEE Proc H 140:455–460
27. Cho MH, Cai W (2010) A wideband fast multipole method for the two-dimensinoal complex Helmholtz equation. Comput Phys Commun 181:2086–2090
28. Schenck HA (1968) Improved integral formulation for acoustic radiation problems. J Acoust Soc Am 44:41–58
29. Burton AJ, Miller GF (1971) The application of integral equation methods to the numerical solution of some exterior boundary-value problem. Proc R Soc Lond A 323:201–210
30. Zheng CJ, Matsumoto T, Takahashi T, Chen HB (2012) A wideband fast multipole boundary element method for three dimensional acoustic shape sensitivity analysis based on direct differentiation method. Eng Anal Boundary Elem 36:361–371
31. Saad Y, Schultz MH (1986) GMRES: a generalized minimal residual algorithm for solving nonsymmetric linear systems. SIAM J Sci Stat Comput 7:856–869
32. Amini S (1990) On the choice of coupling parameter in boundary integral formulations of the acoustic problem. Appl Anal 35:75–92
33. Zheng CJ, Matsumoto T, Takahashi T, Chen HB (2010) Boundary element shape design sensitivity formulation of 3D acoustic problems based on direct differentiation of strongly-singular and hypersingular boundary integral equations. Trans JSME C 76:2899–2908
34. Zheng CJ, Matsumoto T, Takahashi T, Chen HB (2011) Explicit evalution of hypersingular boundary integral equations for acoustic sensitivity analysis by using constant element discretization. Eng Anal Boundary Elem 35:1225–1235
35. Demkowicz L (1994) Asymptotic convergence in finite and boundary element methods. Part 2: The LBB constant for rigid and elastic problems. Comput Math Appl 28(6):93–109
36. Haug EJ, Choi KK, Komkov V (1986) Design sensitivity analysis of structural systems. Academic Press Inc, New York
37. Wolf WR, Lele SK (2011) Wideband fast multipole boundary element method: application to acoustic scattering from aerodynamic bodies. Int J Numer Method Fluids 67:2108–2129
38. Amini S, Prot A (2000) Analysis of the truncation errors in the fast multipole method for scattering problems. J Comput Appl Math 115:23–33
39. Hothersall DC, Chandler-Wilde SN, Hajmirzae NM (1991) The efficiency of single noise barriers. J Sound Vib 146:303–322